JOURNAL OF GEOPHYSICAL RESEARCH, VOL. 113, A00A12, doi:10.1029/2008JA013228, 2008

Interplanetary origin of multiple-dip geomagnetic storms

J. Zhang,[1] I. G. Richardson,[2,3] and D. F. Webb[4]

Received 31 March 2008; revised 31 July 2008; accepted 11 August 2008; published 7 November 2008.

[1] In this paper, we have systematically investigated the interplanetary drivers of major dips during intense ($Dst \leq -100$ nT) geomagnetic storms in 1996–2006. A major dip is defined as a temporary decrease in *Dst* index with amplitude larger than 14.5 nT. Multiple dips result in a storm if regions of geoeffective solar wind with strong southward magnetic fields are separated by less geoeffective solar wind. Among these 90 intense storms, we found that only 34% (31 events) showed a classical "one-dip" profile, while 49% (44 events) had two dips. Another 17% (15 events) had triple or more dips. We found that of a total of 165 major dips associated with the 90 storms, about 45% (74 dips) were caused by interplanetary coronal mass ejections (ICMEs), or ejecta, and 30% (49 dips) were caused by sheaths (SHs) that lie between shocks driven by ICMEs and leading edges of the ICMEs. About 7% (11 dips) were caused by a shock driven by an ICME running into a preceding ICME and intensifying its magnetic field (PICME-SH). About 11% (18 dips) were due to corotating interaction regions (CIRs) formed by the interaction of high-speed solar wind from coronal holes with the preceding slower solar wind. Another 7% (12 dips) were caused by various solar wind structures prior the onset of the storm. Among these different types of drivers, the largest storms dips on average were produced by shocks propagating through preceding ICMEs (PICME-SH). One frequent cause of a two-dip storm is that the first dip is produced by the upstream sheath and the second dip is produced by the driving ICME. Another common cause of a two-dip or multiple-dip storm is the presence of multiple subregions of southward magnetic field within a complex solar wind flow, resulting from two successive, closely spaced ICMEs.

Citation: Zhang, J., I. G. Richardson, and D. F. Webb (2008), Interplanetary origin of multiple-dip geomagnetic storms, *J. Geophys. Res.*, *113*, A00A12, doi:10.1029/2008JA013228.

1. Introduction

[2] A geomagnetic storm is a temporary, substantial energization of the magnetosphere-ionosphere system [*Gonzalez et al.*, 1994]. It is believed that a geomagnetic storm is caused by the intensification of the ring current around the Earth which, through a diamagnetic effect, leads to a decrease in the magnetic field strength at the surface of the Earth. This effect can be quantified through the widely used *Dst* (Disturbance Storm Time) index that is based on the measurements of a set of ground-based magnetometers. The growth of the ring current is due to the injection of energetic ions largely through convection from the plasma sheet, which is known to be driven by the dawn-to-dusk convection electric field (E_Y in GSM coordinates) [*Kozyra and Liemohn*, 2003]. This electric field is generated by the passage of southward directed (B_S) interplanetary magnetic field (IMF) in the solar wind, i.e., $E_Y = V_X B_S$ (where V_X is the component of the solar wind velocity along the Sun-Earth line). Magnetic reconnection between the southward IMF and the oppositely-directed Earth's magnetic field at the magnetopause couples the interplanetary and Earth's magnetic fields. As a result, energy is transferred from the solar wind into the magnetosphere [*Dungey*, 1961].

[3] The classic evolution of a geomagnetic storm has two distinct phases [*Gonzalez et al.*, 1989]. The so-called "main phase" includes the period from storm onset (the initial decrease in *Dst*) to the peak of the storm (time of minimum *Dst*). The "recovery phase" extends from the peak of the storm until *Dst* has recovered to approximately the pre-storm level. Typically, the rate of decrease in *Dst* during the main phase is larger than the rate of increase during the recovery phase. Numerous studies [e.g., *Tsurutani and Gonzalez*, 1997, and references therein] have indicated that when solar wind with a sustained interval of B_S field passes the Earth, the ring current grows. This leads to an intensification of geomagnetic activity that results in *Dst* becoming

[1]Department of Computational and Data Sciences, George Mason University, Fairfax, Virginia, USA.
[2]NASA Goddard Space Flight Center, Greenbelt, Maryland, USA.
[3]CRESST and Department of Astronomy, University of Maryland, College Park, Maryland, USA.
[4]Institute for Scientific Research, Boston College, Boston, Massachusetts, USA.

0148-0227/08/2008JA013228$09.00

more negative and forming the main phase. When the magnetic field turns north or B_S becomes substantially weaker, the loss of energetic ions predominates, leading to the decay of the ring current and a recovery in *Dst*. The relationship between *Dst* and solar wind parameters has been summarized for example by the empirical formulae of *O'Brien and McPherron* [2000].

[4] While many storms show the "classic" *Dst* time profile, with a single minimum that demarcates the main and the recovery phases, it has long been recognized that a significant number of geomagnetic storms have more complicated profiles [e.g., *Tsurutani et al.*, 1988; *Wu and Lepping*, 2002]. *Kamide et al.* [1998] found that about 67% of intense (peak $Dst \leq -100$ nT) and 56% of moderate ($-50 \geq Dst > -100$ nT) geomagnetic storms in their sample of storms showed a double-dip profile, i.e., with two distinct minima. In a recent study, *Richardson and Zhang* [2008] showed that some intense storms in solar cycle 23 evolved in even more complicated ways, with three or even four dips. They concluded that each dip was associated with the passage of a distinct interval of enhanced B_S. Considering the dynamic evolution of storms in the magnetosphere, it is at present unclear whether multiple-dip storms involve "pre-conditioning" of the plasma sheet which may alter the response of the inner magnetosphere to the arrival of subsequent B_S intervals [*Chen et al.*, 2000; *Kozyra et al.*, 2002; *Farrugia et al.*, 2006].

[5] Geomagnetic storms can be caused by a variety of interplanetary structures [*Tsurutani and Gonzalez*, 1997; *Gonzalez et al.*, 1999; *Zhang et al.*, 2007; *Echer et al.*, 2008]. The most common storm drivers are ICMEs. Their internal magnetic fields originate in the region of eruption close to the surface of the Sun that gives rise to the progenitor CME. The magnetic field, as well as the plasma, undergoes rarefaction as the ICME expands en route from the Sun to the Earth. An ICME that generates a storm often has a magnetic cloud (MC) structure, i.e., a flux rope with a smoothly rotating magnetic field [*Klein and Burlaga*, 1982]. Southward fields may be found either in the leading or trailing part of the MC, or close to the center, depending on the orientation of the MC axis [*Lepping et al.*, 1990; *Bothmer and Rust*, 1997; *Wu and Lepping*, 2002]. Another geoeffective structure is the sheath region lying between the shock driven by an ICME and the leading edge of the ICME. Southward field deviations in the sheath may be caused by the southward orientation of the IMF in the solar wind upstream of the shock, which is then compressed at the shock, increasing B_S in the sheath [*Tsurutani et al.*, 1988]. Other causes include magnetic field line draping around the ICME [*McComas et al.*, 1989], Alfvén waves and turbulence [*Tsurutani et al.*, 1995], and the equinoctial projection effect [*Russell and McPherron*, 1973] (see *Gonzalez et al.* [1999] for a summary of these mechanisms). Both the ICME and the accompanying sheath may contribute to the generation of a geomagnetic storm, thus providing one possible scenario for the development of a two-dip storm if both regions include southward fields and they are separated by less geoeffective solar wind (for example, northward field in the leading half of a magnetic cloud are followed by southward fields in the trailing half). Considering their relative geoeffectiveness, *Zhang et al.* [2008] found that on average the ICME contributes about two-thirds of the total energy input into the magnetosphere during a storm while the sheath contributes the other one-third.

[6] More complex solar wind structures, originating from multiple solar CMEs, have been also reported [*Burlaga et al.*, 2002; *Zhang et al.*, 2003; *Xie et al.*, 2006]. These might also be expected to be important generators of multiple-dip storms because of the possibility that multiple B_S intervals may be present, interspersed by regions of less geoeffective solar wind [*Farrugia et al.*, 2006]. One major result achieved through the cooperative efforts at the Living with a Star (LWS) Coordinated Data Analysis Workshops (CDAW) is the identification and the classification of the interplanetary and solar origins of the intense geomagnetic storms in 1996–2005 [*Zhang et al.*, 2007]. The storms were divided into three categories based on their origin: (1) "S-type", resulting from a single ICME, (2) "M-type", caused by multiple ICMEs that interact in interplanetary space, and (3) "C-type", associated with corotating interaction regions (CIRs) [*Belcher and Davis*, 1971; *Smith and Wolf*, 1976] formed at the leading edges of high-speed solar wind flows originating in coronal holes. Among the 88 intense storms studied, 60% (53 events) were S-type, 27% (24 events) M-type, and 13% (11 events) C-type.

[7] In this paper, we will make a systematic study of the *Dst* dips associated with the intense ($Dst \leq -100$ nT) geomagnetic storms that occurred in 1996–2006. *Zhang et al.* [2007] summarized the interplanetary structures responsible for these geomagnetic storms and the possible solar sources. Here, we will use a uniform set of criteria to identify the major temporary decreases (dips) within each storm, and will then classify the type of interplanetary structure responsible for each dip. The improved knowledge of the interplanetary origins of multiple-dip storms will not only help to understand the dynamic processes during the development and decay of a geomagnetic storm, but will also be useful in evaluating the geoeffectiveness of solar eruptions before they reach the Earth. In section 2, we present the method of identification of dips and interplanetary structures. Statistical results are presented in section 3. Discussion and conclusions are given in section 4.

2. Analysis Methods

2.1. Selection of Intense Storms and the Associated Dips

[8] In contrast to *Zhang et al.* [2007], who used visual inspection of the *Dst* index to identify intense storms in which the hourly *Dst* index falls below −100 nT, we select the storms using a computer algorithm. We then use an automated method to identify the major dips within each storm. Because intense storms are relatively infrequent, they are typically well separated from each other in time. However, occasionally, multiple dips that reach the intense storm threshold and are closely spaced in time may occur, in particular during periods of intense solar activity. In such cases, a criterion is needed to distinguish a dip that forms part of an ongoing storm from one that is regarded as a separate storm. *Zhang et al.* [2007] on several occasions assigned two intense dips to form a single intense storm if separated by less than 24 h. Although arbitrary, this turns out to be a reasonable criterion, since in most cases, the two

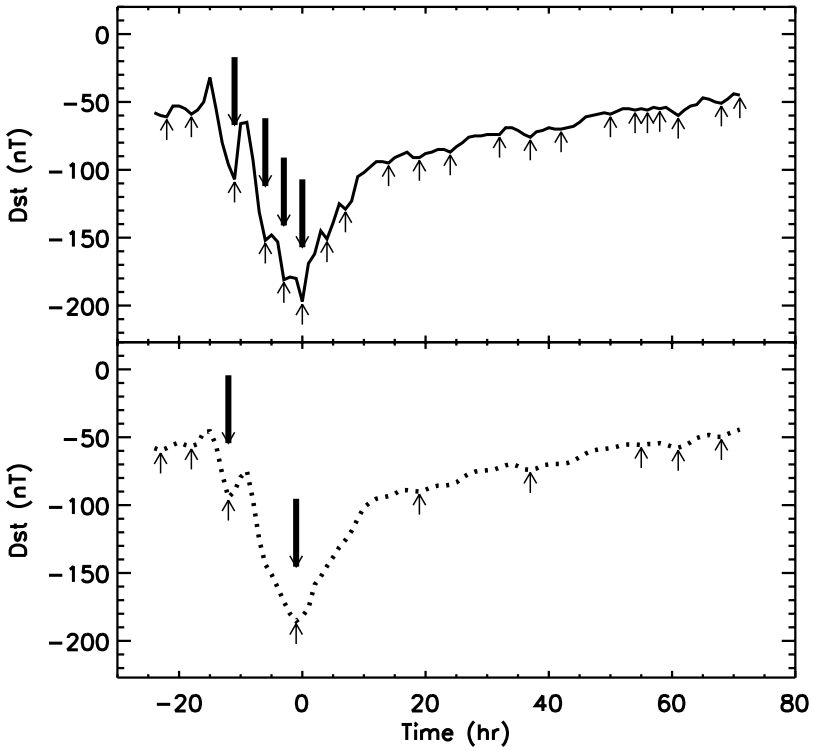

Figure 1. The intense geomagnetic storm (peak $Dst = -197$ nT at 1400 UT on 27 July 2004). (top) The solid line shows the original hourly *Dst* index. The small upward arrows indicate the locations of all dips determined numerically, while the dips indicated by thick downward arrows exceed the intensity threshold for a major dip. (bottom) The dotted line shows the 3-h box-smoothed *Dst* profile. The number of dips is reduced, and only two now exceed the threshold for a major dip, indicating that this storm can be classified as a two-dip storm.

intense dips were generated by an extended solar wind transient, either simple or complex. The automated algorithm to identify intense storms consists of four steps:

[9] 1. Find all instances of $Dst \leq -100$ nT during the study period (1996–2006).

[10] 2. Find the time of minimum *Dst* within 24 h after the time at which the $Dst = -100$ nT threshold is first exceeded; this defines the peak of the storm.

[11] 3. Find the time at which the storm just recovers to above the threshold level, then continue until the time when *Dst* again falls below the threshold.

[12] 4. If these two times (in step 3) are separated less than 12 h, this re-intensification is treated as the continuation of the previous storm. Then repeat Step 3; If the two times are separated by more than 12 h, a new intense storm is found. Then go to Step 2 to find the peak time of the new storm.

[13] This auto-search method yields almost the same list of events as given by *Zhang et al.* [2007] with a few exceptions: (1) The two storms from *Zhang et al.* [2007] peaking at 1200 UT on 6 August 1998 and 0600 UT on 7 August are now treated as one storm. (2) The two storms at 0100 UT and 2300 UT on 30 October 2003 are now regarded as a single storm. (3) Three new storms have been added to the list from *Zhang et al.* [2007]: 1 November 2001, 1100 UT ($Dst = -106$ nT), which was mistakenly excluded owing to the use of provisional *Dst* data when compiling an early version of their list, 5 October 2002, 1600 UT ($Dst = -102$ nT), and 12 November 2004, 1100 UT ($Dst = -109$ nT); these latter two events were previously considered to be part of the ongoing intense activity rather than separate storms.

[14] During 1996–2005, 89 storms are selected using this method, compared to the 88 storms selected and discussed by *Zhang et al.* [2007] during the same period. There was only one intense storm in 2006 to be added ($Dst = -111$ nT at 1000 UT on 14 April). Therefore, 90 intense storms are selected during 1996–2006. Note that the events in 2004–2006 are based on the provisional *Dst* index, so it is possible that they may be slightly adjusted when the final *Dst* index is released.

[15] To identify possible dips associated with a storm, one method is to assess by eye the number of *Dst* dips and then identify the associated structure in the solar wind. However, we have found that this method is highly subjective, with different observers assessing different numbers of dips. To attempt a more objective analysis, we have implemented a computer-based algorithm to select the dips. A dip (i.e., a local minimum) is defined as

$$\begin{aligned} D_i - D_{i-1} &< 0 \\ D_{i+1} - D_i &> 0 \end{aligned} \tag{1}$$

where D is the *Dst* value and the subscript i indicates the time. In Figure 1 (top), we show the *Dst* index for the storm of 27 July 2004, which has a minimum ($Dst = -197$ nT) at

1400 UT. The small arrows indicate 21 dips found using this method during the 96-h period illustrated (24 h prior to and 72 h after storm minimum). However, most of these dips are minor features within the storm. The more important dips can be identified by imposing a depth threshold, where the depth is defined as the difference in *Dst* between the dip minimum and the maximum intensity prior to the dip. For example, a depth threshold of 14.5 nT (this choice will be explained below) reduces the number of dips significantly, to only 4, as indicated by the heavy arrows. Besides the depth threshold, the number of dips also depends on the "smoothness" of the time profile of *Dst*. Figure 1 (bottom) shows the *Dst* profile after applying a 3-h box smoothing filter. On this smoothed profile, only nine dips are found, and only two dips exceed the 14.5 nT intensity threshold.

[16] In this paper, we are interested in the major dips that may be reconciled with coherent interplanetary structures rather than in minor dips. Toward this end, our algorithm chooses dips with the following criteria: (1) The dip appears on the 3-h smoothed *Dst* profile, which is equivalent to the condition that the two dips are separated by more than 3 h used by *Kamide et al.* [1998]. (2) The dip depth should exceed a threshold of 14.5 nT. This value is arbitrary but is the RMS value, or standard deviation, of the 3-h smoothed *Dst* points during 1996–2006 whose value is larger than −50 nT, corresponding, to all periods of quiet conditions or minor geomagnetic activity. (3) The dip should commence within 24 h prior the peak of the storm and within 24 h after the peak of the storm, in order to minimize the overlap with dips associated with other storm events. With these criteria, we found a total of 165 dips associated with the 90 storms. The actual number of dips found by the algorithm depends on the selection of the depth threshold. With a threshold of 10 nT, 190 dips are found, compared with 130 dips for a 20 nT threshold. We should also note that while the 1-minute resolution SYMH index may provide greater information on time variations than *Dst*, we have used *Dst* because we are interested here only in the major dips that have durations of ∼3 h or more.

2.2. Identifying Interplanetary Structures Associated With Major Dips

[17] As discussed by *Zhang et al.* [2007] and *Echer et al.* [2008] and also in earlier studies [e.g., *Tsurutani and Gonzalez*, 1997, and references therein], the structures responsible for intense storms include ICMEs, the sheaths accompanying ICMEs, CIRs and combination of these structures. Using solar wind data obtained from the ACE and WIND spacecraft, we have identified the interplanetary structures responsible for the intense geomagnetic storms and the substructures responsible for the individual dips during these storms. The identification of ICMEs is based on a variety of signatures in the solar wind plasma and magnetic field, including plasma composition/charge state data from the SWICS instrument on ACE (*Zurbuchen and Richardson* [2006] and references therein). We also refer to an updated version of the "comprehensive" ICME list compiled by *Cane and Richardson* [2003] that also considers additional ICME signatures, in particular solar wind ion composition and charge state anomalies [*Lepri et al.*, 2001; *Richardson and Cane*, 2004]. The updated list is available at http://www.ssg.sr.unh.edu/mag/ace/ACElists/ICMEtable.html. For those ICME-related intense geomagnetic storm events, we have looked for shocks driven by the ICMEs and looked into the geoeffectiveness of the resulted sheath regions between shocks and ICMEs. These shocks are fast forward ones, which are recognized by abrupt increase of solar wind velocity, density, temperature and magnetic field (with vary degree of abrupt changes). We have also referred to the ACE shock list compiled by C. W. Smith http://www.ssg.sr.unh.edu/mag/ace/ACElists/obs_list.html) and the WIND and ACE shocks lists compiled by J. Kasper (private communication). CIRs are identified from their characteristic time profiles in the solar wind magnetic field and plasma parameters at 1 AU as described for example by *Belcher and Davis* [1971] and *Schwenn* [1990]. In general, a CIR can be recognized as a compression region with apparently enhanced density and magnetic field, which is preceded by a normal slow stream and followed by a prolonged fast stream; within the compression region, there is often a prominent stream interface indicated by a relatively abrupt depression in the plasma density and increase in the proton temperature and the solar wind velocity. The intense storms in 1996–2004 associated with CIRs, and the related solar wind observations, are discussed by *Richardson et al.* [2006]. In this paper, we identify these substructures responsible for the individual dips during each intense storm. Examples of events with one, two and three dips, as identified by the criteria discussed above, are shown in Figures 2–6.

[18] Figure 2 shows a geomagnetic storm with the classical one-step development, i.e., one single major dip (there are superposed minor dips) with the time of minimum *Dst* indicated by the vertical red line at 1000 UT, 12 August 2000 separating the main and recovery phases. The interplanetary driver of this storm is the passage of an ICME which arrived at 0500 UT on 12 August, as indicated by the black vertical dashed line, and the upstream sheath region extending from the arrival of the ICME-driven shock (11 August, 1810 UT; ACE shock list), indicated by the solid black line, to the ICME leading edge. The sheath/ICME boundary is identified by the decrease in proton temperature below that expected for normal solar wind expansion, shown by the red trace in the T_P panel (see *Richardson and Cane* [1995] for details), and by the increase in solar wind ion charge states and *Mg*/*O* at this time (not shown). (Note these signatures suggest that the ICME extended to 2200 UT on 13 August, indicated by the vertical dotted line although the conspicuous density variations suggest that there may be substructures within this region.) The peak of the storm (*Dst* minimum) is clearly associated with the strong southward magnetic fields reaching ∼30 nT that lie within the leading edge of the ICME. From ∼1300 UT on 12 August, the magnetic field in the ICME is predominantly northward, and *Dst* begins to recover, with no further significant intensification. The sheath region also contributed to the early development of the main phase. In fact, the storm started at about 0200 UT, some 3 h earlier than the arrival of the ICME. Evidently an about 2-h-long duration B_S region in the sheath, reaching around 15 nT, initiated the storm, and caused *Dst* to reach nearly −100 nT. This was followed by a 1-h-long interval of northward-field region, which was immediately followed by the large-scale B_S region in the ICME that led to the peak of the storm. The

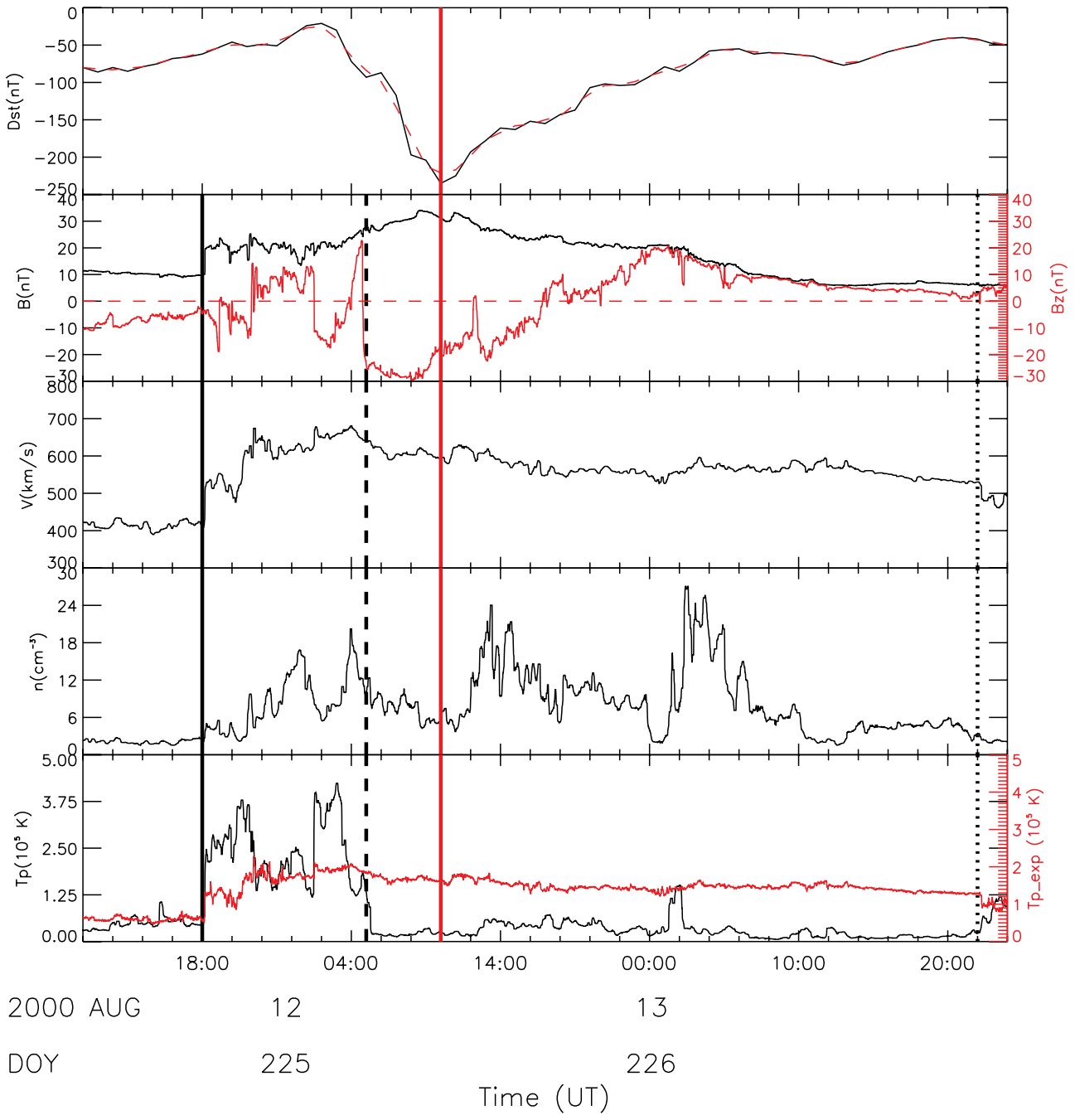

Figure 2. Geomagnetic and interplanetary solar wind data related to the intense geomagnetic storm on 12 August 2000 (peak *Dst* = −235 nT). The five panels from top to bottom show temporal profiles of (1) the *Dst* index (black) overlaid with the result of 3-h box-smoothing (red), (2) the solar wind magnetic field intensity (black) and the B_Z component (red) overlaid, (3) the solar wind velocity, (4) the solar wind density, and (5) the proton temperature (black) overlaid with the expected temperature (red) [*Richardson and Cane*, 1995]. The solar wind data are from ACE in GSM coordinates. The three vertical black lines (solid, broken, and dotted) from left to right indicate the shock arrival time, ICME starting time, and ICME ending time, respectively. The vertical red line indicates the location of the major *Dst* dip. The dip is caused by the ICME in this event. The same format is used for Figures 3–6.

brief non-geoeffective region in the trailing edge of the sheath caused a slight recovery of the storm, as seen in the 1-h *Dst* profile at ~0600 UT. However, the resulting "dip" is averaged out in the 3-h box-smoothed *Dst* profile shown by the red dashed line, and hence is not considered as a major dip by the criteria discussed in the previous section.

[19] Figure 3 shows another example of a one-step storm (peak *Dst* = −105 nT at 0700 UT on January 2005). However, in this case, the main phase is caused by a brief

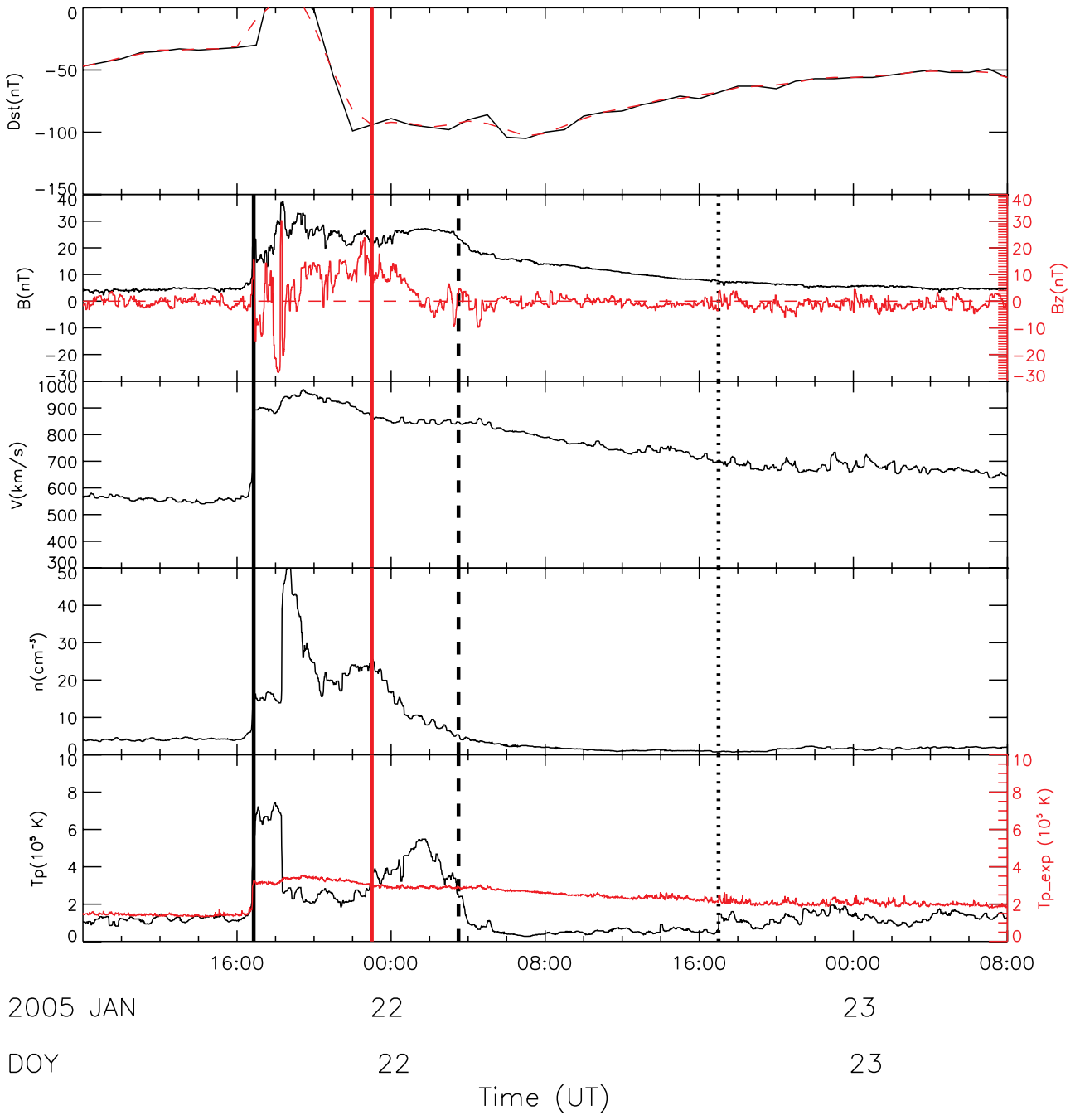

Figure 3. Geomagnetic and interplanetary solar wind data related to the major geomagnetic storm on 22 January 2005 (peak *Dst* = −105 nT). The dip in this storm is caused by the sheath region.

interval of strong, southward magnetic fields in the sheath region following the fast interplanetary shock that passed ACE at 1600 UT on 21 January. The solar wind speed jumped from about ∼550 km/s to ∼900 km/s at the passage of the shock. During the passage of the ICME driving this shock, the storm continued a relatively slow recovery; the ICME did not include any sizable B_S region and hence did not cause any increase in geomagnetic activity.

[20] Figure 4 shows an example of a two-dip storm (peak *Dst* = −182 nT at 1400 UT, 27 July 2004). The first dip was at 0200 UT. The second dip, also the peak of the storm, was 11 h later, at about 1300 UT (the 1-h difference from the storm peak time in the *Dst* index is due to the 3-h box-smoothing applied to *Dst* for detecting dips). Apparently, the first dip was caused by a ∼4 h interval of B_S field in the sheath (from 2200 UT on 26 July to 0200 UT on 27 July). The ICME following the sheath (a magnetic cloud) showed a rotation of the B_Z component from northward to southward over ∼13 h (from 0200 UT to 1500 UT on 27 July). Because of the low geoeffectiveness of the first half of the ICME, *Dst* recovered significantly before the second enhancement, associated with B_S in the second half of the ICME, occurred, forming the two-dip development of this storm.

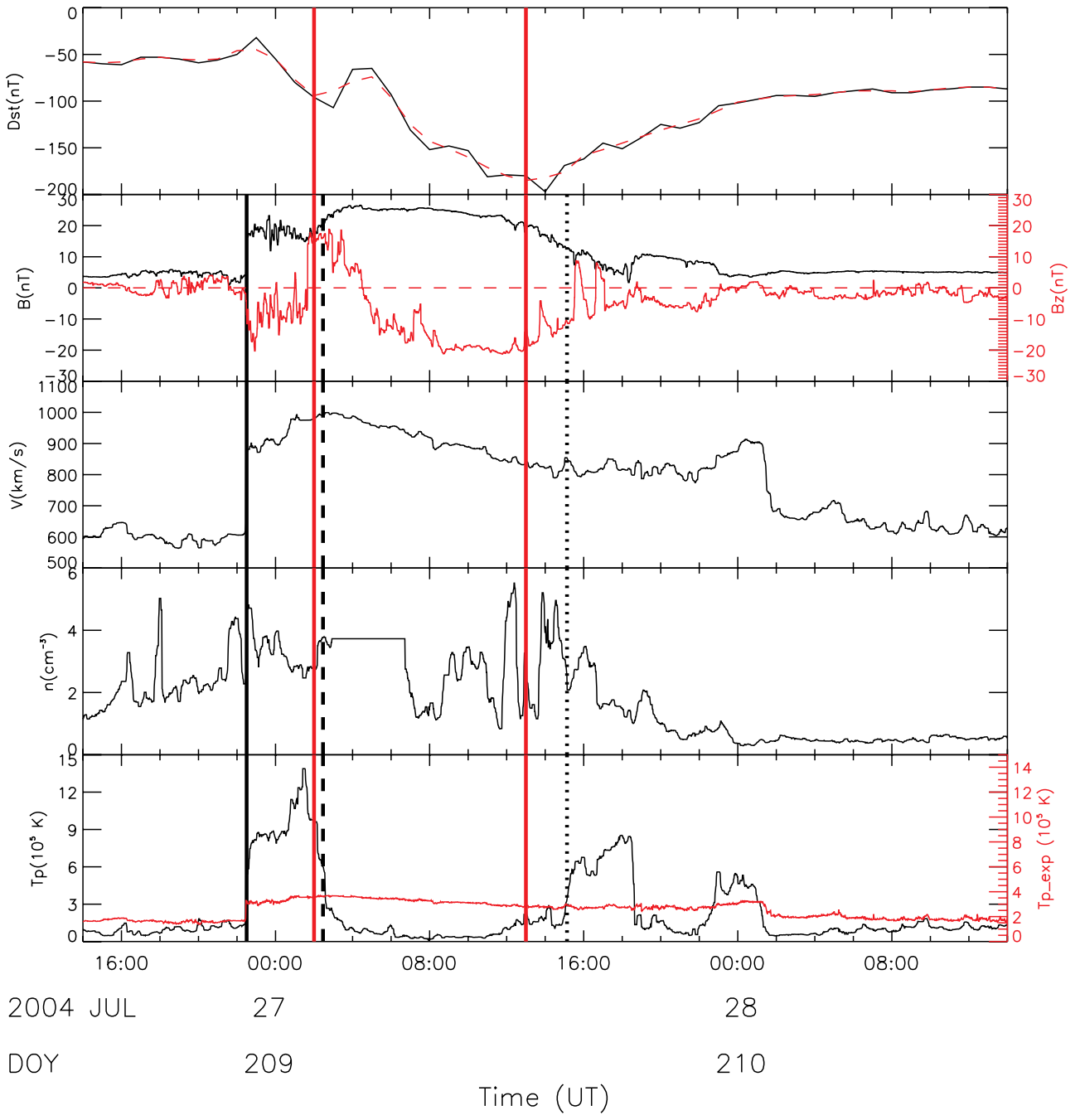

Figure 4. Geomagnetic and interplanetary solar wind data related to the major geomagnetic storm on 27 July 2004 (peak *Dst* = −182 nT). The two dips in this storm are caused by the sheath region and the ICME region.

[21] Figure 5 shows another example of a two-dip storm (peak *Dst* = −181 nT at 0100 UT on 8 September 2002) but with a different interplanetary cause. The first dip was at 2000 UT on 7 September while the second dip was 5 h later, at 0100 UT on 8 September. A shock, observed at 1600 UT on 7 September was propagating through a preceding, unrelated ICME at the time of observation. Evidence for the presence of the preceding ICME includes abnormally low proton temperatures and clear enhancements in solar wind ion charge states observed by the ACE/SWICS instrument(not shown). The magnetic field in the preceding ICME ahead of the shock was southward. Compression by the shock then enhanced the B_S field by a factor of about two, which resulted in the first *Dst* dip. The second dip was caused by a region of southward field in the highly fluctuating sheath. This was also composed of plasma that originated in the preceding ICME based on the continued high ion charge states. The recovery between the first and second dips was due to the existence of a less geoeffective solar wind region (the field turns to the ecliptic briefly) between the two B_S regions within the sheath. The ICME driving the shock was not geoeffective since its magnetic

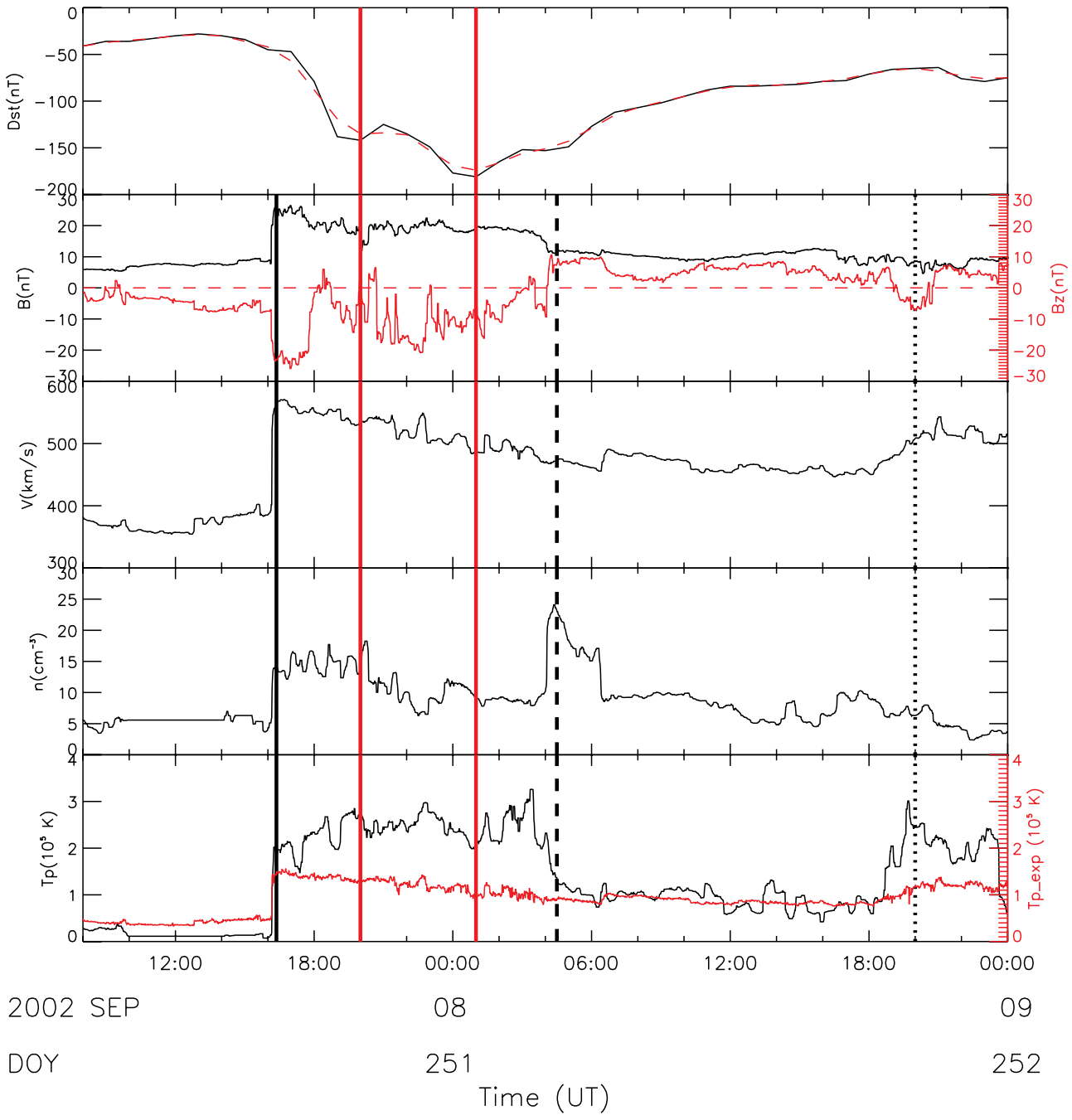

Figure 5. Geomagnetic and interplanetary solar wind data related to the major geomagnetic storm on 8 September 2002 (peak *Dst* = −181 nT). The first dip is caused by a shock running into a preceding ICME. The second dip is caused by the shock sheath.

field was largely northward during the entire duration of the ICME (from about 0400 UT to 2000 UT on 8 September), and hence the storm recovered during passage of the ICME.

[22] Finally, Figure 6 shows an example of a three-dip storm (peak *Dst* = −289 nT at 1000 UT on 10 November 2004). The three dips were at 1600 UT, 2300 UT on 9 November, and 1000 UT on 10 November. This storm followed another intense storm that occurred two days earlier (peak *Dst* = −373 nT at 0700 UT on 8 November). The first dip was caused by the sheath region of the shock arriving at about 0900 UT on 9 November. This shock was also propagating through a preceding, unrelated ICME. However, because the magnetic field in the preceding ICME was northward, the interaction between the shock and the preceding ICME did not raise the level of geomagnetic activity. Instead, the contribution to the first dip was due to the weak but persistent B_S field throughout the fluctuating sheath region. The second dip was associated with the arrival of a second shock at about 1800 UT on 9 November. The strong southward field in the sheath of the shock was

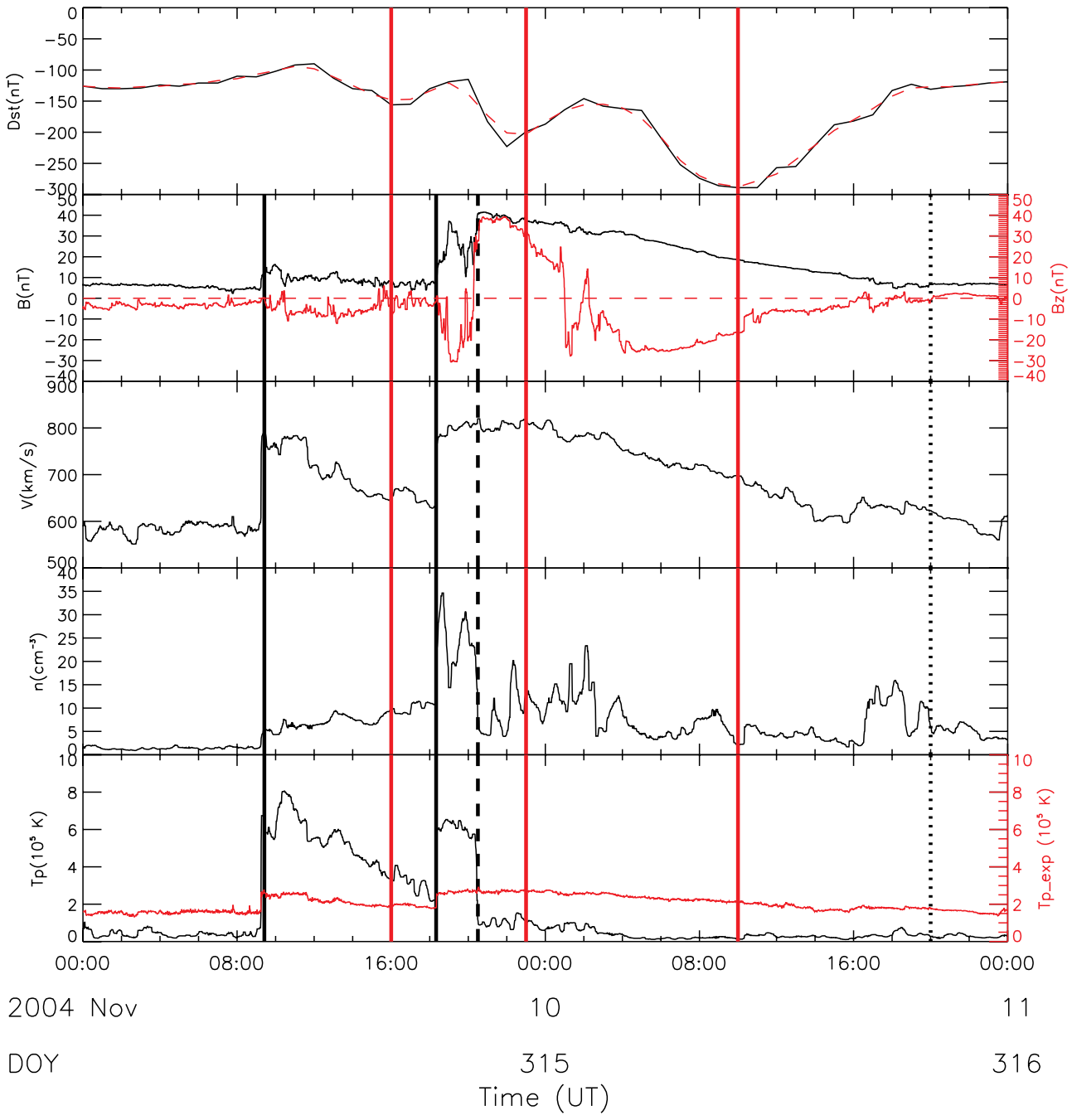

Figure 6. Geomagnetic and interplanetary solar wind data related to the major geomagnetic storm on 10 November 2004 (peak *Dst* = −289 nT). The first two dips are caused by the shock sheath, and the third dip is caused by the ICME. The two vertical solid black lines indicate the presence of two shocks.

probably due to the compression effect of the shock. The third, and largest dip was caused by the ICME which drove the second shock. The ICME (a magnetic cloud) showed a rotation of B_Z from northward to southward. The long separation (about 11 h) between the second and third dips was caused by the presence of an extended region of north-directed field in the first half of the ICME. Thus, the triple-dip development of this storm was associated with two ICME-driven shocks and one of the ICMEs. Consistent with this, solar observations show that the Sun produced multiple front-side halo CMEs a few days prior the storm [*Zhang et al.*, 2007].

3. Statistical Results

[23] We have performed the analysis described above for all the 90 intense storms during 1996–2006. The number of dips in these storms is summarized in Table 1. We find that about one third of these storms (34%; 31 events) have one dip, while around two thirds (66%; 59 events) have two or

Table 1. Number of Dips of Storms and the Interplanetary Driver Types

	All Storms	S-Type	M-Type	C-Type
One-Dip	31 (34%)	18 (32%)	9 (38%)	4 (40%)
Two-Dip	44 (49%)	31 (55%)	9 (38%)	4 (40%)
Three-Dip[a]	15 (17%)	7 (13%)	6 (25%)	2 (20%)
Total	90 (100%)	56 (62%)	24 (27%)	10 (11%)

[a]Including events with three or more dips.

more dips. Among the latter events, 49% (44 events out of all 90 intense storms) have two dips, 16% (14 events) have three dips and 1% (1 event) has four dips. The fractions of one-dip and two-dip storms are similar to those of *Kamide et al.* [1998], who, for a different sample of intense storms, found that 29% had one dip (their "Type 1" storms), and 67% had two dips (their "Type 2"). The remaining 4% were of uncertain type. These independent studies indicate that typically, about one-third of intense geomagnetic storms undergo a classical, one-step development, while about two-thirds of intense storms exhibit a more complicated, two or multiple-step, development. In this study, we have slightly revised the intense storm event list of *Zhang et al.* [2007], as discussed above. Updating the results in that paper, we found that of the 90 intense storms, 62% (56) were "S-type", i.e., caused by a single CME and ICME, 27% (24) were "M-type", associated with multiple ICMEs, and 11% (10) were "C-type", associated with corotating high-speed streams and their related corotating interaction regions.

[24] For the 56 S-type storm events, we found that 32% (18 events) have one dip, 55% (31 events) had two dips, and 13% (7 events) have three dips. These percentages are similar to those found for all events, indicating that S-type events are just as capable of producing intense geomagnetic storms with a multiple-dip development. Regarding the 24 M-type storms, we found that 38% (9 events) had one dip, 38% (9 events) had two dips, and 25% (6 events) had three dips. It is perhaps not surprising that M-type events are more likely to produce triple dip storms than S-type events. For the 10 C-type events, we found that 40% (4 events) had one dip, 40% (4 events) had two dips, and 20% (2 events) had three dips.

[25] In terms of relative intensity of these dips, we found that the first dip had an average *Dst* value of −94 nT, while second dips averaged −145 nT, and third dips −141 nT. The larger second dip compared to the first is consistent with the results presented by *Kamide et al.* [1998] (they did not consider subsequent dips).

[26] Examining the interplanetary structures generating the storm, the number of dips is closely related to the number of distinct B_S structures present, separated by intervals of less geoeffective solar wind. There were 165 major dips identified in the 90 storms studied. The interplanetary drivers of these dips are summarized in Table 2. Nearly a half (45%) of all dips are driven by ICMEs (including magnetic clouds). ICMEs are responsible for 57% of the dips associated with storm main peaks, and for 48% of one-dip storms. Shock sheaths (SH) are the next most important generators of dips, accounting for 30% of all dips, 22% of those associated with storm peaks, and 36% of those associated with one-dip storms. Shocks running through a preceding ICME (PICME-SH) generate 7% of dips, 10% of storm peak dips, and just 3% of one-dip storms. CIRs account for 11% of dips, 11% of storm peak dips and 13% of one-dip storms. In one case, a CIR colliding with a preceding ICME (PICME-CIR) generated a dip. Note that 12 dips (7%) were not assigned to any driver type, and these are designated by "Others" in Table 2. They were caused by activity prior to the onset of the intense storm, usually at the minor or moderate storm level. Nevertheless, these features satisfied the requirement for dips in our automated detection method.

[27] Regarding the relative geoeffectiveness of these interplanetary structures in our sample of intense storms, we found that on average, the most geoeffective structure is PICME-SH, which generates dips with an average minimum value of *Dst* = −161 nT. The second most geoeffective structure is ICME, generating dips with average value of *Dst* = −137 nT, followed by SH (*Dst* = −102 nT). CIRs are the least geoeffective among these structures, with an average dip value of *Dst* = −91 nT.

[28] Considering the 44 two-dip storms (see Table 3), we find that a variety of combinations of solar wind structures are responsible for the two dips. Around a third of two-dip storms (14 events), indicated as (SH, ICME) in Table 3, have a first dip caused by southward magnetic fields during the passage of a shock sheath followed by a second dip associated with an ICME/MC. This situation has been previously noted as a source of two-dip storms [*Kamide et al.*, 1998]. Around a quarter of two-dip storms (10 events) have both dips generated by southward fields in ICMEs, indicated by (ICME,ICME), either in a single ICME (S-type events) or multiple ICMEs [*Farrugia et al.*, 2006]. For only one event, the two dips were caused by two separate B_S intervals within a sheath, indicated by (SH, SH). For about 14% (6) events, one of the two dips was caused by the shock running into a preceding ICME that included southward fields, and the other dip was associated with either an CME (three of the six events), sheath (two events), or CIR (one event). For another 9% (4) events, the two dips were caused by two separate B_S intervals residing in a single CIR, indicated by (CIR, CIR). The other 20% (9) two-dip events were caused by the combination of other structures, such as (SW, ICME) or (SW, SH); "SW" here designates "other" solar wind. In these cases, the first dips were caused by certain solar wind structures prior to the onset of intense

Table 2. Interplanetary Drivers of Storm Dips

Driver	Number	Intensity[a] (nT)	Number[b] (Main-Dip)	Number[c] (One-Dip)
ICME	74 (45%)	−137	51 (57%)	15 (48%)
SH	49 (30%)	−102	20 (22%)	11 (36%)
PICME-SH[d]	11 (7%)	−161	9 (10%)	1 (3%)
CIR	18 (11%)	−91	10 (11%)	4 (13%)
PICME-CIR[e]	1 (1%)	−158		
Others[f]	12 (7%)	−42		
Total	165 (100%)		90 (100%)	31 (100%)

[a]Caused by each type of interplanetary driver.
[b]Only consider the main dip, which is the peak of a geomagnetic storm.
[c]Only considering intense storms with only one major dip.
[d]Shock running into a preceding ICME.
[e]CIR interacting with a preceding ICME.
[f]Typically ahead of the storm onset.

Table 3. Combination of Drivers for Two-Dip Storms

Driver	Dip
(SH, ICME)	14 (32%)
(ICME, ICME)	10 (23%)
(SH, SH)	1 (2%)
(PICME-SH, A)[a]	6 (14%)
(CIR, CIR)	4 (9%)
Others	9 (20%)
Total	44 (100%)

[a]"A" stands for either ICME, SH, or CIR.

geomagnetic storms, and were usually associated with minor activity.

[29] Examining the triple- and quadruple-dip storms, they can be caused "S-type" events as well as "M-type" events. The three-dip storms were generated by a variety of combinations of structures, similar to those producing the two-dip events. These include (SH, SH, ICME), (SH, ICME, ICME) and (ICME, PICME-SH, ICME).

[30] When considering only the main dip associated with the peak of each intense storm, we find that 51 of these 90 dips (57%) were caused by ICMEs, 20(22%) by sheaths, 9 (10%) by PICME-SH, and 10(11%) by CIRs. Compared with all 165 dips, the dips associated with storm peaks are more likely caused by ICMEs than by sheaths.

4. Discussion and Conclusion

[31] The results presented above provide a comprehensive review of the interplanetary drivers of major dips within the 90 intense geomagnetic storms in 1996–2006. The dips are identified after a 3-h smoothing of the hourly *Dst* data and applying a depth threshold of *Dst* = 14.5 nT. About one third of the 90 storms (31; 34%) have one dip, showing the classical development. About two thirds (59; 66%) have two or more dips, showing more complex development. One major cause of the two-dip development is the so-called "sheath-plus-ICME" scenario (for 14 out of the 44 two-dip storms) that has been noted before [*Tsurutani et al.*, 1988; *Kamide et al.*, 1998; *Gonzalez et al.*, 1999; *Wu and Lepping*, 2002; *Zhang et al.*, 2004]. In these cases, both the sheath and the ICME possess strong southward magnetic fields. The region between the two intervals of southward fields must be less geoeffective, in order to produce a partial recovery of *Dst* between the two dips.

[32] However, we have also pointed out several other scenarios that give rise to multiple-dip storms. One important scenario is the passage of two successive ICMEs close in space that may be interacting and merging [*Zhang et al.*, 2003; *Farrugia et al.*, 2006; *Xie et al.*, 2006]. Multiple instances of southward fields may be associated with the sheaths and ejecta of the two driving ICMEs. An interesting situation that involves such an "M-type" event is the propagation of an ICME-driven shock through a preceding ICME that includes southward magnetic fields [*Wang et al.*, 2003; *Farrugia and Berdichevsky*, 2004; *Richardson and Zhang*, 2008]. The compression effect of the shock intensifies the southward magnetic field of the preceding ICME, thus making it much more geoeffective. We found that this preceding-ICME+shock compressing structure on average produces the most intense dips compared to those produced by ICMEs and sheaths alone. Another cause of a two-dip storm is by the irregular field structures within a single ICME, which include two intervals of strong southward fields separated by a less geoeffective region.

[33] A perhaps remarkable result of this study is that "S-type" events have the same probability of producing multiple-dip storms as the "M-type" events. While "M-type" events are more likely to produce triple-dip storms, "S-type" events have a higher probability of generating two-dip storms. Overall, considering the storms associated with both "S-type" and "M-type" interplanetary drivers, about two-thirds are multiple-dip storms, and one-third are single-dip storms. We also note that CIRs may produce two-dip or three-dip storms, depending on the time variability of B_Z in the CIR.

[34] Finally we comment on the dip selection criteria. By using a 3-h smoothing of *Dst* and requiring a threshold on the depth of a dip, we have excluded many smaller dips that are also caused by intervals of southward field in the solar wind [*Richardson and Zhang*, 2008]. Because of the selection of only major dips, and the clear association of these dips with intervals of southward solar wind magnetic fields, it is likely that each dip selected is associated with a sizable intensification of the ring current. Overall, we conclude that multiple-dip development is directly driven by the successive passage of multiple geoeffective structures in the solar wind, instead of internal magnetospheric processes, an alternative possibility noted by *Kamide et al.* [1998]. Nevertheless, the multiple-dip development may involve pre-conditioning of the plasma sheet, which may allow successive geoeffective structures in a sequence to produce a stronger development of the ring current [*Chen et al.*, 2000; *Kozyra et al.*, 2002].

[35] **Acknowledgments.** The ACE plasma and magnetic field data are provided by GSFC Space Physics Data Facility. J.Z. acknowledges the support from NASA grants NNG04GN36G and NNG05GG19G and NSF SHINE grant ATM-0454612. I.G.R. acknowledges a NASA Heliospheric Guest Investigator grant. D.F.W. was supported by AFRL contract FA8718-06-C-0015.

[36] Wolfgang Baumjohann thanks Charles Farrugia and another reviewer for their assistance in evaluating this paper.

References

Belcher, J. W., and L. Davis Jr. (1971), Large-amplitude Alfvén waves in the interplanetary medium: 2, *J. Geophys. Res.*, *76*, 3534–3563.

Bothmer, V., and D. M. Rust (1997), The field configuration of magnetic clouds and the solar cycle, in *Coronal Mass Ejections*, edited by N. Crooker, J. A. Joselyn, and J. Feynman, *Geophys. Monogr. Ser.*, vol. 99, pp. 139–146, AGU, Washington, D. C.

Burlaga, L. F., S. P. Plunkett, and O. C. St. Cyr (2002), Successive CMEs and complex ejecta, *J. Geophys. Res.*, *107*(A10), 1266, doi:10.1029/2001JA000255.

Cane, H. V., and I. G. Richardson (2003), Interplanetary coronal mass ejections in the near-Earth solar wind during 1996–2002, *J. Geophys. Res.*, *108*(A4), 1156, doi:10.1029/2002JA009817.

Chen, M. W., L. R. Lyons, and M. Schulz (2000), Stormtime ring-current formation: A comparison between single-and double-dip model storms with similar transport characteristics, *J. Geophys. Res.*, *105*(A12), 27,755–27,765.

Dungey, J. R. (1961), Interplanetary magnetic field and auroral zones, *Phys. Rev. Lett.*, *6*, 47–48.

Echer, E., W. D. Gonzalez, B. T. Tsurutani, and A. L. C. Gonzalez (2008), Interplanetary conditions causing intense geomagnetic storms ($Dst \leq -100$ nT) during solar cycle 23 (1996–2006), *J. Geophys. Res.*, *113*, A05221, doi:10.1029/2007JA012744.

Farrugia, C., and D. Berdichevsky (2004), Evolutionary signatures in complex ejecta and their driven shocks, *Ann. Geophys.*, *22*, 3679–3698.

Farrugia, C. J., V. K. Jordanova, M. F. Thomsen, G. Lu, S. W. H. Cowley, and K. W. Ogilvie (2006), A two-ejecta event associated with a two-step

geomagnetic storm, *J. Geophys. Res.*, *111*, A11104, doi:10.1029/2006JA011893.
Gonzalez, W. D., B. T. Tsurutani, A. L. C. Gonzalez, E. J. Smith, F. Tang, and S. I. Akasofu (1989), Solar wind-magnetosphere coupling during intense magnetic storms (1978–1979), *J. Geophys. Res.*, *94*, 8835–8851.
Gonzalez, W. D., J. A. Joselyn, Y. Kamide, H. W. Kroehl, G. Rostoker, B. T. Tsurutani, and V. M. Vasyliunas (1994), What is a geomagnetic storm?, *J. Geophys. Res.*, *99*, 5771–5792.
Gonzalez, W. D., B. T. Tsurutani, and A. L. C. Gonzalez (1999), Interplanetary origin of geomagnetic storms, *Space Sci. Rev.*, *88*, 529–562.
Kamide, Y., N. Yokoyama, W. D. Gonzalez, B. T. Tsurutani, A. Brekke, and S. Masuda (1998), Two-step development of geomagnetic storms, *J. Geophys. Res.*, *103*, 6917–6921.
Klein, L. W., and L. F. Burlaga (1982), Interplanetary magnetic clouds at 1 AU, *J. Geophys. Res.*, *87*, 613–624.
Kozyra, J. U., and M. W. Liemohn (2003), Ring current energy input and decay, *Space Sci. Rev.*, *109*, 105–131, doi:10.1023/B:SPAC.0000007516.10433.ad.
Kozyra, J. U., M. W. Liemohn, C. R. Clauer, A. J. Ridley, M. F. Thomsen, J. E. Borovsky, J. L. Roeder, V. K. Jordanova, and W. D. Gonzalez (2002), Multistep Dst development and ring current composition changes during the 4–6 June 1991 magnetic storm, *J. Geophys. Res.*, *107*(A8), 1224, doi:10.1029/2001JA000023.
Lepping, R. P., J. A. Jones, and L. F. Burlaga (1990), Magnetic field structure of interplanetary magnetic clouds at 1 AU, *J. Geophys. Res.*, *95*, 11,957–11,965.
Lepri, S. T., T. H. Zurbuchen, L. A. Fisk, I. G. Richardson, H. V. Cane, and G. Gloeckler (2001), Iron charge distribution as an identifier of interplanetary coronal mass ejections, *J. Geophys. Res.*, *106*(A12), 29,231–29,238.
McComas, D. J., J. T. Gosling, S. J. Bame, E. J. Smith, and H. V. Cane (1989), A test of magnetic field draping induced BZ perturbations ahead of fast coronal mass ejecta, *J. Geophys. Res.*, *94*, 1465–1471.
O'Brien, T. P., and R. L. McPherron (2000), An empirical phase space analysis of ring current dynamics: Solar wind control of injection and decay, *J. Geophys. Res.*, *105*(A4), 7707–7719.
Richardson, I. G., and H. V. Cane (1995), Regions of abnormally low proton temperature in the solar wind (1965–1991) and their association with ejecta, *J. Geophys. Res.*, *100*(A12), 23,397–23,412.
Richardson, I. G., and H. V. Cane (2004), The fraction of interplanetary coronal mass ejections that are magnetic clouds: Evidence for a solar cycle variation, *Geophys. Res. Lett.*, *31*, L18804, doi:10.1029/2004GL020958.
Richardson, I. G., and J. Zhang (2008), Multiple-step geomagnetic storms and their interplanetary drivers, *Geophys. Res. Lett.*, L06S07, doi:10.1029/2007GL032025.
Richardson, I. G., et al. (2006), Major geomagnetic storms ($Dst \leq -100$ nT) generated by corotating interaction regions, *J. Geophys. Res.*, *111*, A07S09, doi:10.1029/2005JA011476.
Russell, C. T., and R. L. McPherron (1973), Semiannual variation of geomagnetic activities, *J. Geophys. Res.*, *78*, 92–108.
Schwenn, R. (1990), Large-scale structure of the interplanetary medium, in *Physics of the Inner Heliosphere I*, edited by R. Schwenn and E. Marsch, pp. 99–181, Springer, New York.
Smith, E. J., and J. W. Wolf (1976), Observations of interaction regions and corotating shocks between one and five AU: Pioneers 10 and 11, *Geophys. Res. Lett.*, *3*, 137–140.
Tsurutani, B. T., and W. D. Gonzalez (1997), The interplanetary causes of magnetic storms: A review, in *Magnetic Storms*, edited by B. T. Tsurutani et al., *Geophys. Monogr. Ser.*, vol. 98, pp. 77–89, AGU, Washington, D. C.
Tsurutani, B. T., W. D. Gonzalez, F. Tang, S. I. Akasofu, and E. J. Smith (1988), Origin of interplanetary southward magnetic fields responsible for major magnetic storms near solar maximum (1978–1979), *J. Geophys. Res.*, *93*, 8519–8531.
Tsurutani, B. T., W. D. Gonzalez, A. L. C. Gonzalez, F. Tang, J. K. Arballo, and M. Okada (1995), Interplanetary origin of geomagnetic activity in the declining phase of the solar cycle, *J. Geophys. Res.*, *100*(A11), 21,717–21,734.
Wang, Y. M., P. Z. Ye, S. Wang, and X. H. Xue (2003), An interplanetary cause of large geomagnetic storms: Fast forward shock overtaking preceding magnetic cloud, *Geophys. Res. Lett.*, *30*(13), 1700, doi:10.1029/2002GL016861.
Wu, C., and R. P. Lepping (2002), Effects of magnetic clouds on the occurrence of geomagnetic storms: The first 4 years of Wind, *J. Geophys. Res.*, *107*(A10), 1314, doi:10.1029/2001JA000161.
Xie, H., N. Gopalswamy, P. K. Manoharan, A. Lara, S. Yashiro, and S. Lepri (2006), Long-lived geomagnetic storms and coronal mass ejections, *J. Geophys. Res.*, *111*, A01103, doi:10.1029/2005JA011287.
Zhang, J., K. P. Dere, R. A. Howard, and V. Bothmer (2003), Identification of solar sources of major geomagnetic storms between 1996 and 2000, *Astrophys. J.*, *582*, 520–533.
Zhang, J., M. W. Liemohn, J. U. Kozyra, B. J. Lynch, and T. H. Zurbuchen (2004), A statistical study of the geoeffectiveness of magnetic clouds during high solar activity years, *J. Geophys. Res.*, *109*, A09101, doi:10.1029/2004JA010410.
Zhang, J., et al. (2007), Solar and interplanetary sources of major geomagnetic storms ($Dst \leq -100$ nT) during 1996–2005, *J. Geophys. Res.*, *112*, A10102, doi:10.1029/2007JA012321.
Zhang, J., W. Poomvises, and I. G. Richardson (2008), Sizes and relative geoeffectiveness of interplanetary coronal mass ejections and the preceding shock sheaths during intense storms in 1996–2005, *Geophys. Res. Lett.*, *35*, L02109, doi:10.1029/2007GL032045.
Zurbuchen, T. H., and I. G. Richardson (2006), In-situ solar wind and magnetic field signatures of interplanetary coronal mass ejections, *Space Sci. Rev.*, *123*, 31–43, doi:10.1007/s11214-006-9010-4.

I. G. Richardson, NASA Goddard Space Flight Center, Code 661, Greenbelt, MD 20771, USA. (ian.g.richardson@nasa.gov)
D. F. Webb, Institute for Scientific Research, Boston College, 140 Commonwealth Avenue, Chestnut Hill, MA 02467, USA. (david.webb.ctr@hanscom.af.mil)
J. Zhang, Department of Computational and Data Sciences, George Mason University, 4400 University Drive, MSN 6A2, Fairfax, VA 22030, USA. (jzhang7@gmu.edu)